Research Article
Geochemistry, Geophysics, Geosystems
DOI 10.1002/2015GC005778

Strain decoupling reveals variable seismogenic risk in SE Japan (Nankai Trough)

James Van Tuyl[1]; Tiago M. Alves[1,*]; Gregory F. Moore[2]

[1]3D Seismic Lab, School of Earth and Ocean Sciences, Cardiff University. Main Building, Park Place, CF10 3AT Cardiff, United Kingdom. Email: alvest@cardiff.ac.uk

[2]Department of Geology & Geophysics, University of Hawaii, 1680 East-West Rd., POST 813, Honolulu, HI 96822, USA

ABSTRACT

The determination of *in situ* stress states is vital in understanding the behavior of faults and subsequent seismogenesis of accretionary prisms. In this paper, a high quality 3D seismic volume is used to map the depth of the extensional-compressional decoupling (ECD) boundary in the accretionary prism of Nankai, with the prior knowledge that strike-slip and compressional stresses occur deeper than 1250 meters below seafloor (mbsf) in the Kumano Basin, changing to extension towards the seafloor. A total of 1108 faults from the accretionary prism are analyzed to estimate paleostresses via fault inversion and slip tendency techniques. A key result is this paper is that the ECD boundary can be used as a proxy to identify active structures on accretionary prisms as its depth depends on: a) local tectonic uplift in areas adjacent to active faults, and b) on the thickness of sediment accumulated above active thrust anticlines. The depth of the ECD boundary ranges from 0 to ~650 mbsf, being notably shallower than in the Kumano Basin. In Nankai, frontal regions of the imbricate thrust zone, and the megasplay fault zone, reveal the shallower ECD depths and correlate with the regions where faulting is most active. As a corollary, this work confirms that estimates of stress state variability based on the analysis of 3D seismic data are vital to understand the behavior of faults and potential seismogenic regions on convergent margins.

This article has been accepted for publication and undergone full peer review but has not been through the copyediting, typesetting, pagination and proofreading process which may lead to differences between this version and the Version of Record. Please cite this article as doi: 10.1002/2015GC005778

Received: Feb 12, 2015; Revised: May 12, 2015; Accepted: May 13, 2015

Keywords: Convergent margins; SE Japan; strain; stress decoupling; seismogenesis; 3D seismic.

1. Introduction

The determination of *in situ* stresses is crucial to understand the accumulation and release of seismic energy in subduction zones [*Lallemand and Funiciello*, 2009]. Local stress distributions reveal key processes governing slip along plate boundary fault systems, and provide information on the regions that are more prone to trigger earthquakes of significant magnitude [*Kinoshita et al.*, 2010; *Kimura et al.*, 2007]. However, the distribution of sub-surface stress is known to vary significantly along and across subduction zones, as demonstrated by *Byrne et al.* [2009] and *Lin et al.* [2010] in the Nankai Trough region (Fig. 1). In particular, Integrated Ocean Drilling Program (IODP) Sites C0002 and C0009 show significant discrepancies in the depth of an extensional-compressional decoupling (ECD) boundary separating a deeper area of compressional and strike-slip stresses from a shallower zone dominated by extension (Figs. 1 and 2). Trying to explain these discrepancies, *Lin et al.* [2010] suggested stress patterns in the proximal Kumano Basin to reflect important strain partitioning during oblique plate convergence [*Lin et al.*, 2010]. The authors also postulated that the magnitude of S_{Hmax} in the accretionary prism of Nankai is higher than that in forearc basin sediments and continental slope deposits.

Notwithstanding the important constraints provided by *Lin et al.* [2010] on a sediment-dominated subduction zone with frequent earthquakes of magnitude 8 and above [e.g., *Ruff and Kanamori*, 1983; *Byrne et al.*, 2009], scarce information on the depth of occurrence of the ECD boundary, and overall stress distribution, is yet available for the accretionary prism of Nankai. Borehole data have been helpful in the recognition of stress distribution in the Kumano Basin, but no methods have been proposed to estimate stress variations at a regional scale. In order to address these caveats, this paper uses a 3D seismic volume from SE Japan to determine the orientation of compressive stresses for thrust and normal faults in the Kumano transect, and thus estimate the

ECD depth across the accretionary prism (Figs. 1 and 2). We combine fault inversion techniques with detailed mapping of the ECD boundary to identify the areas (and structures) of the Nankai accretionary prism in which active faults are predominantly located. Ultimately, this work provides a method to identify regions of subduction zones around the world with the largest seismogenic risk, regardless of a co-seismic, interseismic or post-seismic origin for fault slip and associated slope failure. In more detail, we will test the following hypotheses:

a) The depth of the ECD is not constant within the accretionary prism, thus rendering stress results from IODP Sites C0002 and C0009 valid only locally;

b) Major thrust faults strike favorably for reactivation, and their higher tendency for reactivation is materialized by shallow ECD depths;

c) As a result of b), regions where the ECD is shallowest correlate with the largest seismic activity, and seafloor deformation, in the study area and in other regions of crustal accretion across the world.

2. Data and methods

The IODP NanTroSEIZE expeditions have conducted seismic surveys and drilling programs in the Kumano Transect as part of ongoing investigations into the seismogenesis of SE Japan (Fig. 1). With NanTroSEIZE's scientific support, 3D seismic data covering an area of 12 by 56 km of the Nankai accretionary prism were interpreted in this paper, and 1108 faults analysed on 3D Stress® so that the existence of the ECD boundary could be investigated (Figs. 1b and 2a).

During seismic acquisition, two arrays were used comprising 28 Sodera G-guns (for a volume of 2090 in^3), fired at 37.5 m shot intervals [*Moore et al.*, 2009]. The resulting signal was recorded by an array of four receiver cables, 4500 m long, spaced at intervals of 150 m, with 360 receivers spaced 12.5 m. This geometry provided 8 source-receiver common midpoint (CMP) lines per sail

line at a spacing of 37.5 m and nominal 30-fold data [*Moore et al.*, 2009]. The seismic volume interpreted in this work was pre-stack depth migrated (PSDM) by the Japan Agency for Marine Earth Science and Technology (JAMSTEC). We selected the 3D PSDM volume for our analysis as it provides a clearer image of faults and other small-scale structures not easily recognized in the PSTM seismic volume [*Moore et al.*, 2009].

2.1 *ECD and fault mapping*

The ECD boundary was mapped by identifying the region at depth below which extensional faults do not propagate and thrust faults predominate. The depth at which thrust faulting becomes dominant was mapped manually on Petrel® moving through the seismic volume at intervals of five inlines, i.e. every 72.5 m. To simplify the mapping, and 3D Stress® analyses, the accretionary prism was split in three main regions as outlined in *Moore et al.* [2007]: a) the megasplay fault zone, b) the imbricate thrust zone and, c) the proto-thrust zone (Fig. 2a).

After recognizing the depths in which the lower tips of faults occur, and normal faults change into a region of thrust faults, we mapped the ECD creating a new horizon. A surface was then created in Petrel® using the quick look option in horizon settings.

2.2 3D Stress® modelling

Fault analyzes were performed on 3D Stress® [*Morris et al.*, 1996] to assess the orientation and distribution of compressive and extensional stresses across the Nankai accretionary prism. After mapping 1108 faults, stress inversion techniques were used to determine the principal stress tensors associated with them by following the concepts of *McFarland et al.* [2012]. In *McFarland et al.* (2012), faults striking perpendicular to one of the three principal stresses will not slip, as there is no shear component in this situation (σ_s=0). For any other orientation, σ_s is greater than 0 and frictional

sliding (slip) will occur if σ_s exceeds frictional resistance against slip (Morris et al., 1996). The direction of maximum resolved shear stress controls the type of fault [e.g., *Fossen*, 2010]. If maximum shear stress is in the direction of dip, it will generate normal or reverse faults. If maximum shear stress is horizontal, strike-slip faulting will occur. In any other case oblique-slip will be observed.

Fault populations can be analysed on 3D Stress® relative to fault orientation, lineation trends and sense of slip, which can then be used to calculate the orientation and relative size of the stress tensors (or axes) through stress, or fault-slip, inversions [*Morris et al.*, 1996]. 3D Stress® also evaluates of the quality of these stress tensors based on the degree of agreement between the slip tendency values and corresponding measured displacement values for a set of surfaces. Stress inversion is, therefore, the process of finding the stress state that optimizes this measure of agreement, with the inverted stress tensor being the one that best fits the input fault displacement data [*McFarland et al.*, 2012]. Stress inversions yield four parameters: three unit vectors which specify the orientations of the minimum, maximum and intermediate compressive stress axes, and a scalar describing the relative magnitudes of the principal stresses [*Gephart and Forsyth*, 1984; *Angelier*, 1990]. These parameters provide the current state of stress if faults are still active or, instead, the paleostress state at the time of formation of the faults. *McFarland et al.* [2012] state that two important criteria need to be considered when assessing the quality of fit for the stress tensors. Based on the agreement between slip tendency and observed displacement at measured surfaces, the criteria are: a) a positive relationship between slip tendency and displacement is expected; b) small displacements with large slip tendency are more plausible than large displacements with small slip tendency, i.e. surfaces may have started slipping at different points in time.

2.3. Slip tendency analyses

Slip tendency (T_s) analysis is a technique that allows rapid assessment of stress states and related potential fault activity [*Morris et al.*, 1996]. It is based on:

a) The ability to calculate the state of normal and shear stress for a fault or fracture of any orientation within a stress tensor [*Ramsey*, 1967];

b) The assumption that the resolved shear and normal stresses on a surface are strong predictors of both the likelihood and direction of slip on that surface [*Wallace*, 1951; *Bott*, 1959; *Lisle and Srivastava*, 2004].

Slip is driven by the resolved shear stress (T), and occurs when T equals or exceeds the frictional resistance of sliding (*F)*, which is proportional to the normal stress, σ_n, acting across the surface [*Jaeger and Cook*, 1979; *Morris et al.*, 1996; *Lisle and Srivastava*, 2004] such as:

$$T_{Critical} = \mu\sigma_{n'} \quad (2)$$

with μ representing coefficient of sliding friction (with no units) and σ_n' the normal stress acting on a plane, in MPa. Slip tendency (T_s) is the likelihood that a fault will slip and is calculated from the ratio between shear stress (T) and normal stress (σ_n'). Slip tendency and direction varies across planes with different orientations, as documented in this work.

3. Geological setting

3.1. Late Cenozoic evolution of the Nankai Trough

The Nankai subduction zone comprises an active convergent margin located in SE Japan where subduction of the Philippine Sea plate beneath the southwest margin of the Eurasian Plate occurs at

a convergence rate of ~4.1-6.5 cm/yr, with an azimuth of ~300^{o} to 315^{o} [*Seno et al.*, 1993; *Miyazaki and Heki*, 2001; *DeMets et al.*, 2010; *Moore et al.*, 2013] (Fig. 1a). Subduction offshore Nankai is associated with back-arc spreading processes behind the Izu-Bonin arc complex, and has been occurring since the middle Miocene [*Nakamura et al.*, 1984*; Okino et al.*, 1994]. The relatively shallow nature of the Nankai Trough is due in part to subduction of young shallow Shikoku Basin crust, and to the thick sediment cover of the subducting plate [*Moore et al.*, 1990]. This sediment-dominated subduction zone has led to the accumulation of a thick accretionary prism, several hundred kilometers wide [*Kinoshita et al.,* 2010; *Kopf et al.,* 2010], constrained to the northwest by the Kumano Basin and to the southeast by the Shikoku Basin (Fig. 1b).

The accretionary prism of Nankai consists of accreted and underplated trench-fill turbidite facies [*Kinoshita et al.*, 2010; *Kopf et al.*, 2010], transported axially along the Nankai Trough as a result of subduction of the Izu-Bonin arc during the Pliocene-Pleistocene [*Taira and Niitsuma*, 1986]. Hemipelagic mudstones and volcanic ash from the Shikoku Basin have also been drilled [*Moore et al.*, 1990; *Brown et al.*, 2003]. Sediments within the Nankai accretionary prism are preferentially deformed via thrust faulting, folding and volume loss [*Tobin and Kinoshita*, 2006; *Moore et al.*, 2007; *Gulick et al.*, 2010; *Moore et al.*, 2013]. In contrast, sediments below the basal décollement remain relatively unaffected [*Bangs et al.*, 2009; *Tobin and Saffer*, 2009].

3.2 Morphology of the study area

In the shallower part of the accretionary prism outboard of the Kumano Basin, thrust packages are overthrust by a younger, first-order fault system that extends over 120 km along strike [*Park et al.*, 2002; *Moore et al.*, 2007; 2009]. This megasplay fault system is a major out-of-sequence splay fault located landward from the imbricate thrust zone [*Bangs et al.*, 2009; *Martin et al.*, 2010]. Branching upwards from the plate boundary thrust, approximately 50 km landward of the trench, the megasplay fault cuts discontinuously through the accretionary prism and separates the active

outer accretionary prism from the inner prism [*Park et al.*, 2002; *Moore et al.*, 2009; *Kimura et al.*, 2011].

In the interpreted 3D seismic volume, branches of the megasplay fault are visible cutting through the outer accretionary prism (Fig. 2a). Coseismic slip occurs along some of the branches of the megasplay fault, including outwards from the plate boundary mega-thrust into the frontal décollement, to produce a number of great earthquakes [*Fukao* 1979; *Baba et al.*, 2006; *Hamada et al.*, 2015]. In fact, the outer accretionary prism of Nankai exhibits a long history of seismogenesis [*Byrne et al.*, 2009] and associated tsunamis [*Ando*, 1975]. Frequent large thrust earthquakes of magnitudes (M) eight and above on the richter scale, such as the 1944 Tonankai M8.2 and Nankaido M8.3 earthquakes [*Ando*, 1975; *Ruff and Kanamori*, 1983; *Kinoshita et al.*, 2010] occur along the plate boundary, making it one of the best studied active margins in the world [*Byrne et al.*, 2009]. Thrust earthquakes at the Nankai subduction zone occur at shallow depths within subduction zone [*Li*, 2011].

Oceanward from the megasplay fault zone are observed a series of imbricate thrusts (Fig. 2a). Here, bathymetric data shows a ridge-basin topography [e.g., *Morley*, 2009], with seafloor deformation marked by east-northeast trending hanging-wall anticlines to the east and southward dipping monoclines to the west [*Kimura et al.*, 2011; *Alves et al.*, 2014]. Large thrust faults striking southwest are shown cutting upwards from a décollement at depth, while the uppermost sediments are cut by northwest to west-northwest striking oblique normal faults [*Kimura et al.*, 2011].

The deeper proto-thrust zone is characterized by a relatively flat seafloor in water depths between 4500 m and 4900 m [*Moore et al.*, 1990], where trench turbidites overlie Shikoku basin hemipelagic mudstones accreted from the subducting oceanic plate [*Taira and Ashi*, 1993] (Fig. 2a). The proto-thrust zone is a zone of diffuse structural thickening between the deformation front and the frontal thrust. It reflects a zone of intense tectonic deformation where the décollement initially develops. Consequently, the proto-thrust zone is heavily faulted with both landward and seaward dipping thrust faults (Fig. 2a).

3.3 The NanTroSEIZE project and previous stress state results

The IODP NanTroSEIZE project has acquired seismic and borehole data in the Kumano Basin and adjacent accretionary prism in an attempt to understand the mechanics of seismogenesis and rupture propagation along subduction plate boundary faults [*Tobin et al.*, 2009; *McNeill et al.*, 2010]. The new data provided the opportunity to estimate *in situ* stress state orientations landward from the megasplay fault zone by interpreting compressive failures (borehole breakouts), drilling-induced tensile fractures and anelastic strain recovery data at IODP Site C0002 [*Chang et al.*, 2009; *Tobin et al.*, 2009] and IODP Sites C0009, C0006, C0004, and C0001 [*Lin et al.*, 2010] (Fig. 1).

Stress orientations at IODP Site C0002 are parallel to the plate boundary and interpreted as reflecting strike-slip faulting (Fig. 1b). In contrast, at IODP Site C0009 stress orientations are orthogonal to the plate boundary. This contrast in stress orientations was interpreted to mark an effective decoupling at ~1250 mbsf between stresses in the strata above, where extension is prevalent, and strata below where compression is dominant [Lin et al., 2010; Sacks et al., 2013] (Fig. 2b). As a result, Lin et al. [2010] proposed that the regional stress pattern reflects strain partitioning during oblique plate convergence. Depth-dependent strength [*Chéry et al.*, 2004] along the shelf edge proximal to IODP Site C0002 caused a rotation of stresses toward a more parallel direction to the plate boundary [*Martin et al.*, 2010; *Lin et al.*, 2010].

The relationship between the ECD and structural styles interpreted on seismic was recently established by *Saffer et al.* [2013], *Sacks et al.* [2013], *Lewis et al.* [2013] and *Moore et al.* [2013]. The authors identified a series of normal fault populations at IODP Site C0002, and demonstrated that shallow sediments in the Kumano Basin are subject to extension, which is also the youngest mode of faulting [*Park et al.*, 2002; *Gulick et al.*, 2010; *Lewis et al.*, 2013; *Moore et al.*, 2013]. Recorded S_{Hmax} orientations at IODP Site C0002 are consistent with dominant extension, with two

phases of normal faulting relating to a) continuing thrusting within the underlying accretionary prism, and b) stretching perpendicular to the regional convergence vector [*Moore et al*., 2013; *Sacks et al.*, 2013]. After performing stress inversions for normal faults in the Kumano Basin, *Sacks et al.* [2013] showed that the calculated direction of maximum horizontal extension documents a rotation over time that is consistent with the present-day horizontal principal stress orientations determined from wellbore failures and anelastic strain recovery at IODP Sites C0002 and C0009 [*Chang et al.*, 2010; *Byrne et al.*, 2009; *Lin et al.*, 2010; *Moore et al.*, 2013]. This rotation of stresses with depth represents the change from a normal faulting regime in the upper few kilometers to a compressional regime in the prism interior [*Chang et al.*, 2010; *Moore et al.*, 2013; *Lin et al.*, 2010]**,** and correlates with the zone of strain partitioning at ~1250 mbsf first observed by *Lin et al.* [2010] (Fig. 2b).

4. Results

4.1. 3D modelling of thrust faults

4.1.1. Megasplay fault zone

A number of branches of the megasplay fault are visible cutting up through the accretionary prism (faults A to D; Fig. 2a). Faults A to D are large features and laterally continuous. At depth they become discontinuous and increasingly difficult to map due to lower seismic resolution.

Faults A to D dip to the northwest between 27^{o} and 32^{o}. Fault C is relatively steeper, dipping at 36^{o}. All faults are shallower dipping than equivalent thrusts in the imbricate thrust zone (Fig. 2a). Thrust faults strike to the northeast, parallel to the Nankai Trough axis.

Stress inversion for faults A to D shows stress configurations that agree with oblique thrust faulting in the megasplay fault zone (Fig. 3a). In faults A and D, σ_2 is near horizontal. In faults B and D, σ_1 strikes N123 and N128. This latter azimuth is roughly parallel to the present-day

convergence vector. Faults A and C show maximum directions of compression (σ_1) at N95^o and N156^o respectively, suggesting oblique thrusting in the two structures (Fig. 3a).

Slip direction along fault B exhibits near vertical slip directions. The stereograph in Fig. 3a documents slip directions clustered to the northwest slightly oblique to the N128 convergence vector. In addition, Fig. 4a shows high slip tendency across most of fault B, with values reaching more than 0.643. As documented later in this work, high slip tendencies are not limited to the deeper structural levels in faults A to D, indicating that branches of the megasplay fault are highly active across their entire surface. This characteristic contrasts with faults in the imbricate-thrust and proto-thrust zones.

In essence, the shallower dip of thrust faults in the megasplay fault zone generates relatively high slip tendencies where the faults approach the seafloor, with the maximum slip focused around σ_3 along planes dipping 10^o to 30^o. The 3D seismic volume does not image megasplay thrust faults soling out, thus preventing the modeling of slip tendencies at depth. However, we expect the observed trend of increased slip tendency with depth to continue in thrust faults A to D that sole out as they enter deeper structural levels (Fig. 2a).

4.2.2. Imbricate thrust zone

Thrust faults in the imbricate thrust zone cut upwards from a basal décollement zone to shallow structural levels, generating imbricate thrust packages with associated anticlines (Fig. 2a). Thrust faults 1 to 4 strike between N232 and N253^0, near parallel to the trench axis. Fault dips range from 32^o to 39^o, and are notably lower than those documented in the proto-thrust zone (Fig. 2a). Fault dips decrease as they approach the basal décollement.

Stress inversion data show faults 2, 3 and 4 with compressive stress configurations that agree with Andersonian thrust faulting [*Anderson*, 1951], whereas fault 1 shows a tendency for strike-slip

movement. The orientation of the maximum compressive stress (σ_1), for all thrust faults is near parallel to a convergence vector of N300-315^o (Fig. 3b).

Modelling of thrust faults in the imbricate thrust zone show maximum slip tendency to be focused at depth, where the fault angles decrease as thrusts sole into the décollement (Fig. 4b). In this latter figure is shown data for fault 2 as an example of the slip tendencies recorded in this zone. Such a character suggests that faults have greater amounts of cumulative slip at depth. As the faults become steeper, notably as they propagate onto the surface, slip tendency decreases and the faults lock at shallower levels.

4.2.3 Proto-thrust zone

Thrust faults in the proto-thrust zone are mostly landward dipping (Fig. 2a). They offset subducting Shikoku basin sediments and exhibit highly variable lateral continuity and depth. Faults in this zone strike parallel to the trench axis (N234^o), and are steeply dipping (~62^o). Stress inversion data denote oblique thrust faulting in agreement with Anderson [1951], with σ_1 horizontal and parallel to the current convergence vector of 300-315^o [*DeMets et al.*, 2010] (Fig. 3c).

Slip direction in the proto-thrust zone is predominantly sub-vertical, striking northeast–southwest in the direction of convergence (Fig. 4c). The stereograph in this figure shows two clear slip vector clusters either side of σ_3, where slip tendency is greatest. Slip vectors show marked variations when fault dips and strikes change towards the surface.

Slip tendency is highly variable across proto-thrust fault II, with values between 0.0 and 0.520 for a fluid pressure of 0 MPa (Fig. 4c). Slip tendency is relative low across proto-thrust fault II in comparison to the imbricate thrust zone and megasplay fault, which commonly show values higher than 0.270 (Fig. 4). This contrast in maximum slip tendency values suggests that thrust faults in the proto-thrust zone are relatively stable.

4.3. Normal faulting and the ECD in the accretionary prism

4.3.1 Normal fault distribution

Normal fault populations are predominantly confined to young accretionary prism sediments. They are often observed on the flanks of thrust anticlines, cutting up to shallow structural levels (Fig. 5a). In these cases, the ECD depth profile shows a characteristic shallowing where thrust faults approach the seafloor. Normal faults in the megasplay fault zone are steeply dipping, and restricted to very shallow structural levels of 200 to 300 mbsf (Fig. 5a). Normal faults are seaward dipping and frequently interact with branches of the megasplay that cut up to the seafloor. Normal faults are restricted vertically and laterally, and are small features compared to the larger thrusts below.

Normal faults within the imbricate thrust zone occur in young slope sediments, in the perched basin and shallow accretionary prism sediments located on the backs of anticlinal structure (Fig. 5b). Normal faults show a variety of strikes across the imbricate thrust zone, but no normal fault populations occur in the proto-thrust zone. This character suggests strata are not subject to extension in the proto-thrust zones, which is rather dominated by thrust faulting under a compressive regime (Fig. 5a).

In contrast to the Kumano basin, the ECD boundary occurs in the accretionary prism at a much shallower depth and is highly variable along the length of the accretionary prism (Figs. 5a and 5b). A seaward shallowing trend is visible in the ECD boundary, surfacing short of the frontal thrust slope and proto-thrust zone (Fig. 5a).

The extensional-compressional decoupling is at its deepest below a perched basin located between the megasplay and the imbricate thrust zones (Figs. 2a and 5a). Normal fault populations are common throughout the basin sediments and the ECD boundary is visible dropping to a maximum depth of ~650 mbsf before shallowing sharply (Fig. 6a)**.** Landward of the perched basin,

337 the ECD boundary shallows again reaching depths of 0 mbsf to 200 mbsf (Fig. 6a). Notably, the boundary approaches the seafloor where branches of the megasplay fault cut up to the surface, and surface sediments are thin. This character is also visible in parts of the imbricate thrust zone, namely where thrust faults propagate vertically to the seafloor (Figs. 5a, 5b and 6a).

The imbricate thrust zone shows a highly fluctuating depth profile for the ECD boundary, with depth increasing between thrust anticlines, i.e. where perched slope basins have formed (Fig. 5a). In turn, the ECD boundary approaches very shallow depths where the near-seafloor sediment is thin, and normal faults are relatively scarce.

6. DISCUSSION AND CONCLUSIONS

6.1. Significance and distribution of strain decoupling in the accretionary prism

Results from 3D Stress® inversion reveal older accretionary prism sediments to have been subjected to horizontal shortening in the proto-thrust zone, imbricate thrust zone and along branches of the megasplay fault zone. These results are in agreement with observations in *Lewis et al.* [2013], *Chang et al.* [2010] and *Lin et al.* [2010], in which maximum horizontal compressive stress (σ_1) is deemed parallel to the convergence vector within the older accretionary prism sediments. However, our results are not in agreement with data from IODP Site C0002, where trench parallel σ_1 was perpendicular to the trench axis, suggesting predominant strike-slip movements associated with the megasplay fault [*Chang et al.* 2010; *Lin et al.* 2010].

The depth of the ECD boundary is shallower within the accretionary prism, and exhibits greater variability compared to the Kumano Basin (Fig. 5a). This character is particularly noted along branches of the megasplay, where 3D Stress® fault inversions show σ_1 to be horizontal and mostly parallel to the convergence vector (Fig. 3). Significantly, if trench-parallel maximum horizontal compressive stress is representative of the older accretionary sediments within the Kumano Basin, it

indicates a change in tectonic regime either side of the megasplay. Trench-parallel maximum horizontal compressive stress at IODP Site C0002 could be the result of strain partitioning in the form of a transtensional strike-slip fault system associated with the Kumano Basin Edge Fault Zone [*Martin et al.*, 2010].

In this research, 3D Stress® models show maximum horizontal compressive stress (σ_1) parallel to the convergence vector and perpendicular to maximum horizontal compressive stress at IODP Site C0002. The landward region of the accretionary prism is not subject to extension but rather compression, a result that agrees with *Lewis et al.* [2013], in which stress inversions determined thrusts at IODP Site C0002, and shallow drill cores within overthrust sediments associated with the megasplay (IODP Site C0001) exhibit σ_1 perpendicular to the trench. Thus, 3DStress® results not only provide evidence for strain partitioning between the megasplay fault and the Kumano Basin Edge Fault Zone in line with *Martin et al.* [2010], but also show that stress orientations at IODP Site C0002 determined by *Lin et al.* [2010] are not representative of current stress states within the accretionary prism.

6.2. Does modeling slip and fluid flow across accretionary prisms, constitute a valid method to identify seismically active structures?

Faults in the imbricate thrust zone show strike-slip and normal fault geometries chiefly located on the landward limbs of thrust anticlines. While not a conventional location for extensional faulting, it is apparent from seismic data that extension occurs through brittle fracturing of weak near-seafloor strata above the thrust anticlines during their deformation. This character suggests that the stress orientations of these normal faults are dominated by the proximity of thrust faults to the surface and landsliding of slope sediments [*Strasser et al.*, 2011], leading to a relatively shallowing of faults on the continental slope. The variation in principal stress orientations between groups of normal faults within the imbricate thrust zone as well as those associated with the megasplay fault

zone lends weight to the argument that young sediments above the decoupling boundary have not yet accommodated the regional stress recorded within accretionary prism strata (Fig. 6b). Rather, they are responding to local stress fields produced by thrust along faults in the accretionary prism. Therefore, it could be said that extension on top of thrust anticlines is occurring in response to localized critical taper, influenced by thrusting and the relative shallowing of thrust faults below.

As a result, we interpret that ECD depth variations in the study area relate to thrust fault activity and subsequent erosion of thrust anticlines and pop-up structures, produced by movement along major thrust faults (Fig. 6b). This setting is chiefly noted at the toe of the accretionary prism, where faults are recognisingly active due to intense compression generated by the subducting slab. In parallel, the relative increase of sediment flux to the toe recorded at present may require enhanced thrusting in the attempt towards forming a critical taper. Recent fault activity is also documented along the megasplay fault in the form of slope failure in the shallowest parts of this structure [*Kimura et al.*, 2011].

Using the methodology in this paper, regions of accretionary prisms can therefore be classified according to the relative fault activity they present, based on the depth of the ECD boundary. The frontal part of the imbricate thrust zone and the megasplay are revealed as the regions of highest fault activity and, potentially, largest seismogenic risk - if assuming coseismic slip for most of the structures interpreted in the study area. This assumption is valid in light of recent data in *Hamada et al.* [2015], which recognized slow slip velocity, long-term rise time, and large displacement are recognized both the megasplay fault zone and the frontal décollement. These parameters were considered by the authors to be longer and slower than typical coseismic slip, but are rather consistent with rapid afterslip. The trenchward section of the imbricate thrust zone is close behind in terms of its fault activity, while thrust faults beneath the perched basin are of relatively low activity. In a wider context, this method could be applied to the greater extent of the Nankai accretionary prism, as well as to other subduction zones, given appropriate 3D seismic data coverage.

Acknowledgements

This research used 3D seismic data provided by the Integrated Ocean Drilling Program (IODP). The data are available at the UTIG seismic data repository (http://www.ig.utexas.edu/sdc/cruise.php?cruiseIn=kumano3d). Schlumberger provided the Petrel® software package used to interpret the seismic data in this work. SWRI's 3D Stress® was used in the fault analyses presented here. We thank S. Gulick and G-Cubed editor-in-chief Thorsten Becker for their reviews.

7. REFERENCES

Alves, T. M., Strasser, M., and Moore, G.F. (2014), Erosional features as indicators of thrust fault activity (Nankai Trough, Japan), *Marine Geology*, 356, 5–18, http://dx.doi.org/10.1016/j.margeo.2013.07.011.

Anderson, E.M. (1951). *The Dynamics of Faulting and Dyke Formation with Application to Britain* (2nd Edn), Oliver and Boyd, Edinburgh.

Ando, M. (1975), Source mechanism and tectonic significance of historical earthquakes along the Nankai Trough Japan, *Tectonophysics*, 27, p119-140.

Angelier, J. (1990), Inversion of field data in fault tectonics to obtain the regional stress – III.A new rapid direct inversion method by analytic means, *Geophysical Journal International*, 103, 363-376, doi:10.11111/j.1365-246X.1990.

Baba, T., Cummins, P.R., Hori, T., and Kaneda, Y. (2006), High precision slip distribution of the 1944 Tonankai earthquake inferred from tsunami waveform: Possible slip on a splay fault, *Tectonophysics*, 426, p119-134, doi:10.1016/j.tecto.2006.02.015

Bangs, N.L.B., Moore, G.F., Gulick, S.P.S., Pangborn, E.M., Tobin, H.J., Kuramoto, S. and Taira, A. (2009), Broad, weak regions of the Nankai Megathrust and implications for shallow coseismic slip, *Earth and Planetary Science Letters*, 284, 44–49.

Bott, M.H.P. (1959), The mechanics of oblique slip faulting, *Geological Magazine*, 96, 109-117.

Brown, K.M., Kopf, A., Underwood, M.B., and Weinberger, J.L. (2003), Compositional and fluid pressure controls on the state of stress on the Nankai subduction thrust: A weak plate boundary, *Earth and Planetary Science Letters*, 214, 589-603.

Byrne, T.B., Lin, W., Tsutsumi, A., Yamamoto, Y., Lewis, J.C., Kanagawa, K., Kitamura, Y., Yamaguchi, A., and Kimura, G. (2009), Anelastic strain recovery reveals extension across SW Japan subduction zone, *Geophysical Research Letters*, 36, L23310, doi:10.1029/2009GL040749.

Chang, C., et al. (2009), Constraining in situ stress tensor in the Kumano forearc basin, Nankai, based on borehole wall failure analysis, *Eos Trans. AGU 90(52)*, Fall Meet. Suppl., Abstract T21C-1832.

Chang, C., McNeill, L.C., Moore, J.C., Lin, W., Conin, M., and Yamada, Y. (2010), In situ stress state in the Nankai accretionary wedge estimated from borehole wall failures. *Geochemistry, Geophysics, Geosystems*, 11, Q0AD04, doi:10.1029/20101GC003261.

Chéry, J., Zoback, M.D., Hickman, S. (2004), A mechanical model of the San Andreas fault and SAFOD Pilot Hole stress measurements, *Geophysical Research Letters*, 31, L15S13, doi:10.1029/2004GL019521.

DeMets, C., Gordon, R.G., and Argus, D.F. (2010), Geologically current plate motions, *Geophysical Journal International*, 181, p1-80, doi:10.1111/j.1365-246X.2009.04491.x

Fossen, H. (2010), *Structural Geology*, Cambridge University Press, Cambridge, 189-201.

Fukao, Y. (1979), Tsunami earthquakes and sudubtion processes near deep-sea trenches, *Journal Geophysics Results*, 84, 2303-2314, doi:10.1029/JB084IB05P02303.

Gephart, J.W. and Forsyth, D. (1984), An improved method for determining the regional stress tensor using earthquake focal mechanisms data: application to the San Fernando earthquake sequence, *Journal of Geophysical Research*, 89, 9305-9320.

Gulick, S.P.S., Bangs, N,L.B., Moore, G.F., Ashi, J., MArtin, K.M., Sawyer, D.S., Tobin, H.J., Juramoto, S., and Taira, A. (2010), Rapid forearc basin uplift and megasplay fault development

from 3D seismic images of Nankai Margin off Kii Peninsula, Japan*, Earth and Planetary Science Letters*, 300, 55–62.

Hamada, Y., Sakagushi, A., Tanikawa, W., Yamagushi, A., Kameda, J. and Kimura, G. (2015), Estimation of slip rate and fault displacement during shallow earthquake rupture in the Nankai subduction zone, *Earth, Planets and Space*, 67:39, doi: 10.1186/s40623-015-0208-0.

Ito, Y., Asano, Y., and Obara, K. (2009), Very-low-frequency earthquakes indicate a transpressional stress regime in the Nankai accretionary prism, *Geophysical Research Letters*, 36, L20309, doi:10.1029/2009GL039332.

Jaeger, J.C. and Cook, N.G.W. (1979), Fundamentals of rock mechanics (third edition). London, United Kingdom, Chapman and Hall, 593pp.

Kimura, G., Kitamura, Y., Hashimoto, Y., Yamaguchi, A., Shibata, T., Ujiie, K., and Okamoto, S. (2007), Transition of accretionary wedge structures around the up-dip limit of the seismogenic subduction zone, *Earth and Planetary Science Letters,* 225(3–4):471-484. doi:10.1016/j.epsl.2007.01.005

Kimura, G., Moore, G.F., Strasser, M., Screaton, E., Curewitz, D., Streiff, C., and Tobin, H. (2011), Spatial and temporal evolution of the megasplay fault in the Nankai Trough, *Geochemistry, Geophysics, Geosystems*, 12, Q0A008. http://dx.doi.org/10.1029/2010GC003335.

Kinoshita, M., Tobin, H., Eguchi, N. and Nielsen, S. (2010), Integrated Ocean Drilling Program Expedition 326 Scientific Prospectus. doi:10.2204/iodp.sp.326.2010. Available at http://publications.iodp.org/scientific_prospectus/326/326sp_5.htm

Kopf, A., Strasser, M., Monsees, N., Underwood, M.B. and Guo, J. (2010), Data report: particle size analysis of sediments recovered during IODP Expeditions 315 and 316, Sites C0001 – C0008, Nankai Trough forearc, off Japan. doi:10.2204/iodp. Proc. 314315316.207.2011. Available at http://publications.iodp.org/proceedings/314_315_316/207/207_.htm. Last accessed: 14th March 2014.

Lallemand, S. and Funiciello, F. (2009), *Subduction Zone Geodynamics*, Springer, Berlin.

Lewis, J.C., Byrne, T.B. and Kanagawa, K. (2013), Evidence for mechanical decoupling of the upper plate at the Nankai subduction zone: Constraints from core-scale faults at NantroSEIZE sites C0001 and C0002, *Geochemestry, Geophysics, Geosystems*, 14, 620-633, doi:10.1029.2012GC004406

Li, C-F. (2011), An integrated geodynamic model of the Nankai subduction zone and neighboring regions from geophysical inversion and modelling, *Journal of Geodynamics*, 51, 64-80.

Lin, W., Doan, M.L., Moore, J.C., McNeill, L. et al. (2010), Present-day principal horizontal stress orientations in the Kumano forearc basin of the southwest Japan subduction zone determined from IODP NanTroSEIZE drilling site C0009, *Geophysical Research Letters*, 37, L13303, doi:10.1029/2010GL043158.

Lisle, R.J. and Srivastava, D.C. (2004), Test of the frictional reactivation theory for faults and validity, of faults-slip, *Geology*, 32, 569-572, doi:10.1130/G20408.1

Martin, K.M., Gulick, S.P.S., Bangs, N.L.B., Moore, G.F., Ashi, J., Park, J.-O., Kuramoto, S. and Taira, A. (2010), Possible strain partitioning structure between the Kumano fore-arc basin and the slope of the Nankai Trough accretionary prism, *Geochemistry, Geophysics, Geosystems*, 11, Q0AD02, doi:10.1029/2009GC002668.

McFarland, J.M., Morris, A.P. and Ferrill, D.A. (2012), Stress inversion using slip tendency, *Computers and Geosciences*, 41, 40-46.

McNeill, L., Saffer, D., Byrne, T., Araki, E., Toczko, S., Eguchi, N., Takahashi, K. and IODP Expedition 319 Scientists (2010), IODP Expedition 319, NanTroSEIZE Stage 2: First IODP Riser Drilling Operations and Observatory Installation Towards Understanding Subduction Zone Seismogenesis. Scientific Drilling, 10, doi:10.2204/iodp.sd.10.01.2010.

Miyazaki, S., and Heki, K. (2001), Crustal velocity field of southwest Japan: subduction and arc-arc collision, *Journal of Geophysical Research*, 106(B3), 4305–4326. doi:10.1029/ 2000JB900312

Moore, G.F., Shipley, T.H., Stoffa, P.L., Karig, D.E. et al. (1990), Structure of the Nankai Trough Accretionary Zone From Multichannel Seismic Reflection Data, *Journal of Geophysical Research*, 95, No.B6, 8753-8765.

Moore, G.F., Bangs, N.L., Taira, A., Kuramoto, S., Pangborn, E. and Tobin, H.J. (2007). Three-Dimensional splay fault geometry and implications for tsunami generation, *Science*, 318, 1128-1131.

Moore, G.F., Park,J.SO., Bangs, N.L., Gulick, S.P., Tobin, H.J., Nakamura, Y., Sato, S., Tsuji, T., Yoro, T., Tanaka, H., Uraki, S., Kido, Y., Sanada, Y., Kuramoto, S., and Taira, A. (2009), Structural and Seismic data stratigraphic framework of the NanTroSEIZE Stage 1 transect. In Kinoshita, M., Tobin, H., Ashi, J., Kimura, G., Lallemant, S., Screaton, E.J., Curewitz, D., Masago, H., Moe, K.T., and the Expedition 314/315/316 Scientists, (2009) Proceedings of IODP legs 314/315/316: Washington, DC (Integrated Ocean Drilling Program Management International, Inc.). 2–3, doi:10.2204/iodp.proc.314315316.102.2009

Moore, G.F., Boston, B.B., Sacks, A.F. and Saffer, D.M. (2013), Analysis of normal fault populations in the Kumano Forearc Basin, Nankai Trough, Japan: 1. Multiple orientations and generations of faults from 3-D coherency mapping, *Geochemistry, Geophysics, Geosystems*, 114, 1989-202, doi:10.1002/ggge.20119.

Morley, C. (2009), Growth of folds in a deep-water setting, *Geosphere*, 5, 59-89. http://dx.doi.org/10.1130/GES00186.1.

Morris, A.P., Ferrill, D.A. and Henderson, D.B. (1996), Slip tendency analysis and fault reactivation, *Geology*, 24, 275-278.

Nakamura, K., Shimazaki, K. and Yonekura, N. (1984), Subduction, bending and eduction – Present and Quaternary Tectonics of the northern border of the Philippine Sea plate, *Bulletin de la Societe Geologique de France*, 26, 221-243.

Okino, K., Shimakawa, Y. and Nagaoka, S. (1994), Evolution of the Shikoku Basin, *Journal of Geomagnetism and Geoelectricity*, 46, 463-479.

Park, J.O., Tsuru, T., Kodaira, S., Cummins, P.R. and Kaneda, Y. (2002b), Splay fault branching along the Nankai subduction zone, *Science*, 297, 1157-1160.

Ramsey, J.G. (1967), *Folding and fracturing of rocks*, New York. McGraw Hill, p560.

Ruff, L. and Kanamori, H. (1983), Seismic coupling and uncoupling at subduction zones, *Tectonophysics*, 99(2–4), 99-117, doi:10.1016/0040-1951(83)90097-5

Sacks, A., Saffer, D.M and Fisher, D. (2013), Analysis of normal fault populations in the Kumano forearc basin, Nankai Trough, Japan: 2. Principal axes of stress and strain from inversion of fault orientations, *Geochemistry, Geophysics, Geosystems*, 14, 1973-1988.

Saffer, D.M. et al. (2013), In situ stress and pore pressure in the Kumano forearc basin, offshore SW Honshu from down-hole measurements during riser drilling, *Geochemistry, Geophysics, Geosystems*, doi:10.1002/ggge.20051.

Seno, T., S. Stein and A. E. Gripp (1993), A model for the motion of the Philippine Sea plate consistent with NUVEL-1 and geological data, *Journal of Geophysical Research*, 98, 17941–17948.

Taira, A. and Niitsuma, N. (1986), Turbidite sedimentation in the Nankai Trough as interpreted from magnetic fabric, grain size, and detrital model analyses. Available at: http://www.deepseadrilling.org/87/volume/dsdp87_12.pdf Last accessed: 26th March 2014.

Tobin, H.J. and Kinoshita, H.J. (2006), NanTroSEIZE: the IODP Nankai trough seismogenic zone experiment, *Scientific Drilling*, 2, 23–27.

Tobin, H.J. and Saffer, D.M. (2009), Elevated fluid pressure and extreme mechanical weakness of a plate boundary thrust, Nankai Trough Subduction zone, *Geology*, 37, 679-682. Doi:10.1130/G25752A.1

Wallace, R.E. (1951), Geometry of shearing stress and relationship of faulting, *Journal of Geology*, 59, 111-130.

Figure captions

Figure 1. a) Inset showing the tectonic setting of SE Japan. The study area is shown by the red box. b) Shaded relief map of the Nankai Trough regions showing the location of IODP Sites (black dots) and stress data interpreted at each site. Red lines through marked drilling sites indicate maximum horizontal stress directions (Byrne et al., 2009; Chang et al., 2010; Lin et al., 2010). Blue line at IODP Site C0002 indicates maximum horizontal stress directions in sediments shallower than 936 m below seafloor. Yellow arrows mark the convergence vector between the Philippines Sea plate and SE Japan (Seno et al., 1993; Heki, 2007). Black lines indicate maximum horizontal stress directions for sediments above the ECD, as estimated in this paper. White lines indicate maximum horizontal stress directions for strata below the ECD. Note that IODP Site C0002 shows maximum stress in older accretionary prism strata to be near trench-parallel, a character suggesting strike-slip faulting in that particular region of the Nankai slope (Moore et al., 2013).

Figure 2. a) Interpreted PSDM seismic inline 2440 showing the main structural zones, and structures, in the Nankai accretionary prism. Dashed black line marks the top of the oceanic basement, as interpreted in this work. Black solid lines indicate major thrust faults, with dashed lines marking the discontinuous character of megasplay fault branches. Dashed red line marks the basal décollement onto which the thrust faults sole out. Vertical Exaggeration = 1.5x. b) PSDM seismic inline 2455 from the Kumano Basin, showing IODP Sites C0002 and C0009 and normal faults crossing the youngest sediment, as interpreted by Sacks et al. (2013). Note that normal faults populations cut down to the top of the older accretionary prism sediments but do not propagate below a boundary of structural decoupling. Red line highlights the structural decoupling boundary interpreted by Lin et al. (2010), where a change from extensional to a compressional regime occurs at a depth of around 1250mbsf. IBT-Izu-Bonin Trench; KRP-Kyushu-Palau Ridge; KP-Kii Peninsula; FSC-Fossil Spreading Center; PSP-Philippine Sea Plate.

Figure 3. a) Results of stress inversion for thrust faults A, B, C and D in the megasplay fault zone, plotted on a stereograph showing slip tendency. Faults show compressive stresses (σ_1, σ_2 and σ_3) concordant with the Andersonian criteria (Anderson 1951) for thrust faulting. Stress tensor σ_1 strikes near-parallel to the convergence vector on all faults, with thrust fault A marginally oblique. Stereographs show slip tendency to be greatest (Red) on planes dipping at low angles to the northwest. Rows within the table beneath each stereograph show the azimuth, dip and relative magnitudes from top to bottom of σ_1, σ_2 and σ_3. b) Stress inversion results of thrust faults 1, 2, 3 and 4 in the imbricate thrust zone. The configuration of faults 2, 3 and 4 show oblique thrust faulting, while fault 1 shows strike-slip faulting. In all cases σ_1 is horizontal and near parallel to the convergence vector, although thrust faults show variation. The boxes below each stereograph show the azimuth, plunge and magnitude of each fault, for σ_1, σ_2 and σ_3 (top to bottom). Color scheme of stereograph shows slip tendency, with highest slip tendencies on planes dipping are low angles to the northwest. c) Results of stress inversion for thrust faults I, II, III and IV in the proto-thrust zone, plotted on a stereograph showing slip tendency. Faults show compressive stresses (σ_1, σ_2 and σ_3) concordant with the Andersonian criteria for thrust faulting (Anderson 1951). In the stereographs, σ_1 strikes near-parallel to the convergence vector on all faults, with thrust fault I marginally oblique. Stereographs show slip tendency to be greatest (red color) on planes dipping at low angles to the northwest. Rows within the table beneath each stereograph show the azimuth, dip and relative magnitudes from top to bottom of σ_1, σ_2 and σ_3.

Figure 4. a) Slip direction and tendency values for thrust megasplay branch B. Slip vectors are vertical across the fault, striking north-northwest to south-southeast. Stereograph color scheme shows slip tendency with planes exhibiting maximum slip around σ_3 and shallow dipping to the northwest. b) Slip direction and tendency values across fault 2 in the imbricate thrust zone. Slip direction (white arrows) across thrust fault 2 is sub-vertical, parallel to the orientation of σ_1, northeast southwest. Overall, stereographs show greatest leakage factor to occur on planes whose

poles are around σ_3. c) Slip directions and tendency across proto-thrust fault II. Slip directions are oblique to the fault plane. Such a distribution of vectors documents a NW-SE slip direction. Stereogram on the right-and side shows slip tendency for the faults imaged in the figure.

Figure 5. Interpreted PSDM seismic line 2440 showing interpreted fault populations and the interpreted ECD depth. In the accretionary prism, the ECD shows a shallower depth than that interpreted by Lin et al. (2010) in the Kumano Basin. The depth of the ECD is highly variable and varies between 0 m and ~650 mbsf. Vertical Exaggeration = 1.5x. b) Interpreted ECD depth in a perched slope basin in the accretionary prism (see Fig. 1b for location of PSDM seismic inline 2440). Note the variable depth of the ECD in this region, a character interpreted to correlate with the presence of tectonically active structures, and associated erosion of seafloor strata.

Figure 6. a) Depth map of the ECD relative to the seafloor, as interpreted in this paper. b) Summary of the effects of erosion of accretionary prisms on the depth of the ECD and distribution of normal fault families. Thrust faults generate the pop-up structures responsible for the irregular geometry of the ECD. Structural highs are then subject to erosion as the accretionary prism tries to retain critical taper. The subsequent removal of seafloor sediment and the exhumation of older accretionary prism strata results in the ECD to approach shallow depths above active thrust faults and associated anticlines.

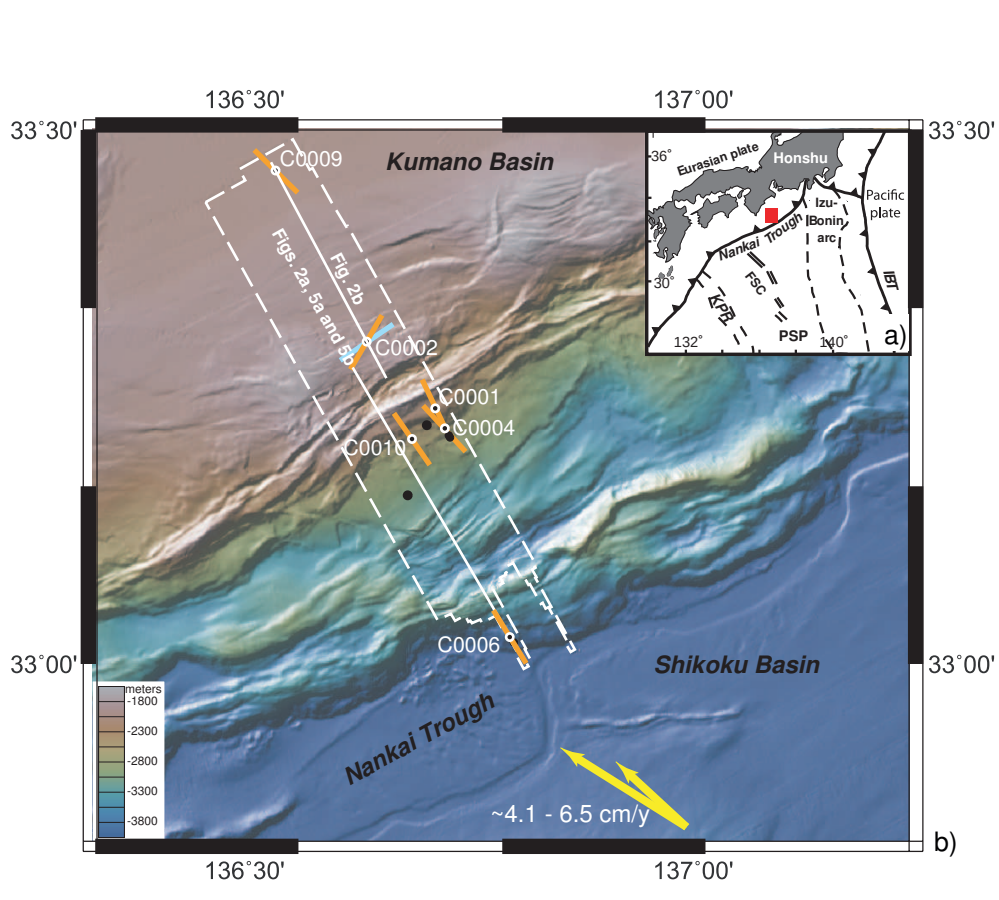

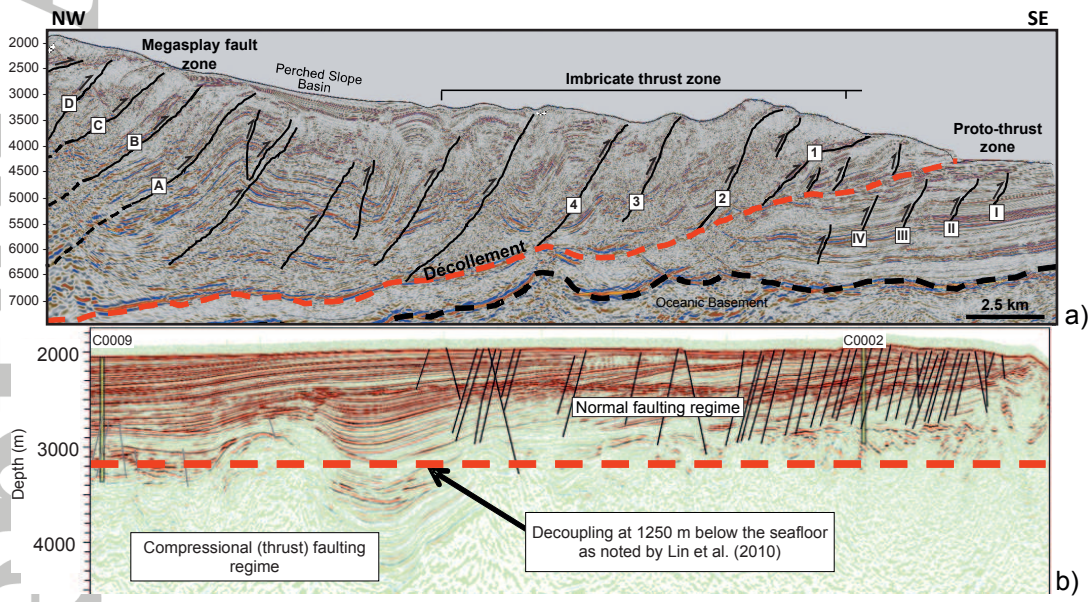

Megasplay fault

Imbricate thrust zone (ITZ)

Proto-thrust zone

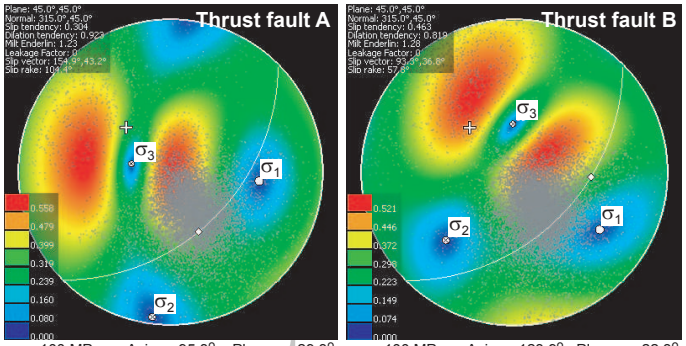

= 100 MPa Azim = 95.8° Plunge = 29.3°
= 58.87 MPa Azim = 7.3° Plunge = -2.6°
= 34.45 MPa Azim = 101.8° Plunge = -60.5°

σ_1 = 100 MPa Azim = 123.9° Plunge = 22.3°
σ_2 = 64.46 MPa Azim = 45.2° Plunge = -25.6°
σ_3 = 36.80 MPa Azim = 178.2° Plunge = -54.9°

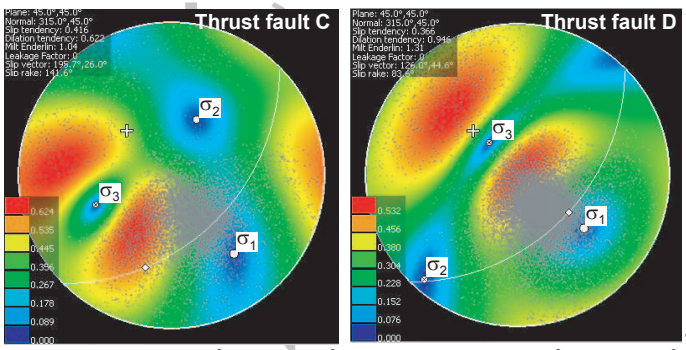

a)

= 100 MPa Azim = 141.5° Plunge = 23.5°
= 67.07 MPa Azim = 24.1° Plunge = 46.6°
= 30.79 MPa Azim = 68.6° Plunge = -34.0°

σ_1 = 100 MPa Azim = 128.8° Plunge = 31.3°
σ_2 = 54.09 MPa Azim = 41.6° Plunge = -4.5°
σ_3 = 36.09 MPa Azim = 138.9° Plunge = -58.3°

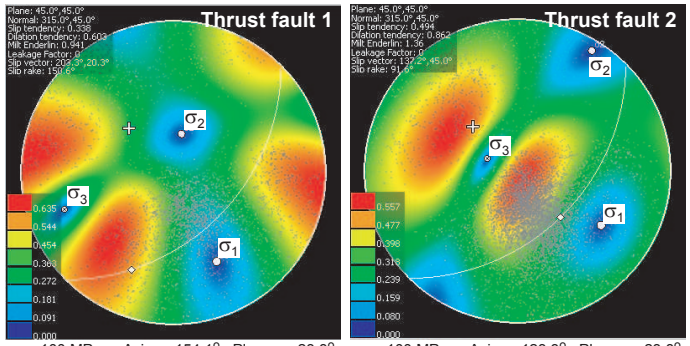

σ_1 = 100 MPa Azim = 154.1° Plunge = 23.8°
σ_2 = 61.40 MPa Azim = 11.8° Plunge = 60.9°
σ_3 = 30.20 MPa Azim = 71.3° Plunge = -15.8°

σ_1 = 100 MPa Azim = 123.3° Plunge = 23.8°
σ_2 = 57.51 MPa Azim = 31.5° Plunge = 4.2°
σ_3 = 34.56 MPa Azim = 112.2° Plunge = -65.8°

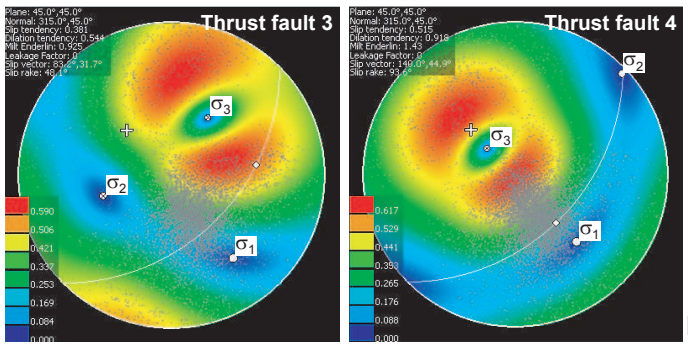

b)

σ_1 = 100 MPa Azim = 143.4° Plunge = 21.8°
σ_2 = 73.63 MPa Azim = 73.1° Plunge = -40.0°
σ_3 = 32.62 MPa Azim = 212.3° Plunge = -42.1°

σ_1 = 100 MPa Azim = 137.8° Plunge = 28.3°
σ_2 = 77.32 MPa Azim = 46.6° Plunge = 2.2°
σ_3 = 31.12 MPa Azim = 132.5° Plunge = 61.6°

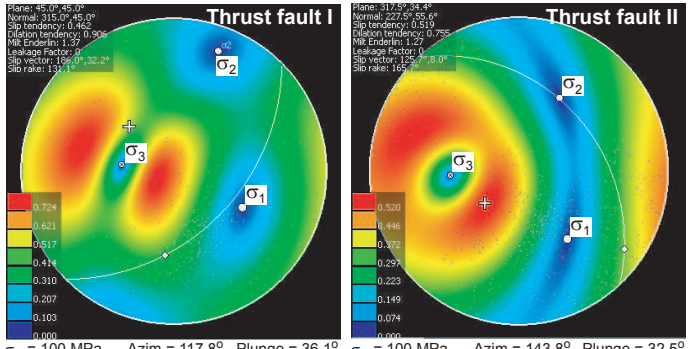

σ_1 = 100 MPa Azim = 117.8° Plunge = 36.1°
σ_2 = 59.23 MPa Azim = 20.3° Plunge = 20.3°
σ_3 = 26.05 MPa Azim = 97.1° Plunge = -52.1°

σ_1 = 100 MPa Azim = 143.8° Plunge = 32.5°
σ_2 = 85.71 MPa Azim = 29.8° Plunge = 32.5°
σ_3 = 36.83 MPa Azim = 86.7° Plunge = -40.5°

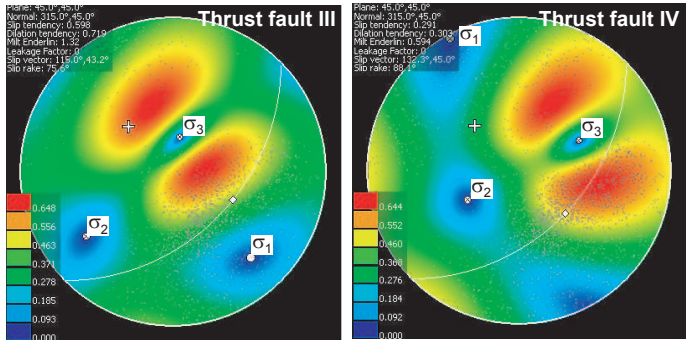

c)

σ_1 = 100 MPa Azim = 137.7° Plunge = 15.9°
σ_2 = 57.98 MPa Azim = 53.5° Plunge = -19.6°
σ_3 = 29.53 MPa Azim = 191.2° Plunge = -64.4°

σ_1 = 100 MPa Azim = 152.2° Plunge = -1.5°
σ_2 = 65.58 MPa Azim = 60.5° Plunge = -47.5°
σ_3 = 29.73 MPa Azim = 243.6° Plunge = -42.4°

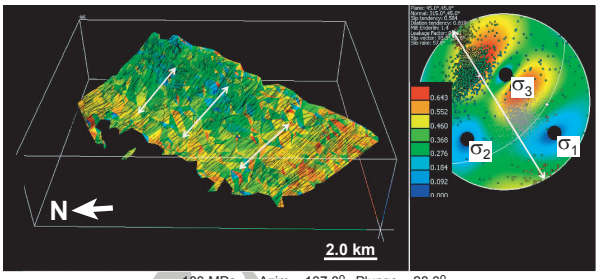

a)

σ_1 = 100 MPa Azim = 137.8° Plunge = 28.3°
σ_2 = 77.32 MPa Azim = 46.6° Plunge = 2.2°
σ_3 = 31.12 MPa Azim = 132.5° Plunge = -61.6°

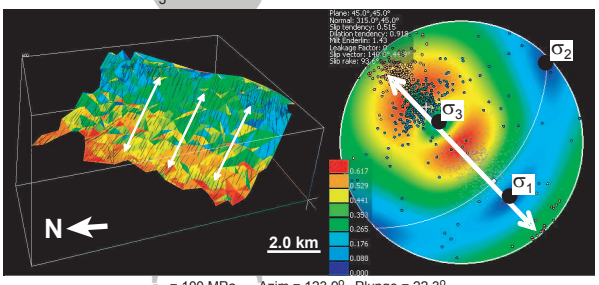

b)

σ_1 = 100 MPa Azim = 123.9° Plunge = 22.3°
σ_2 = 54.44 MPa Azim = 45.2° Plunge = -25.6°
σ_3 = 26.80 MPa Azim = 178.2° Plunge = -54.9°

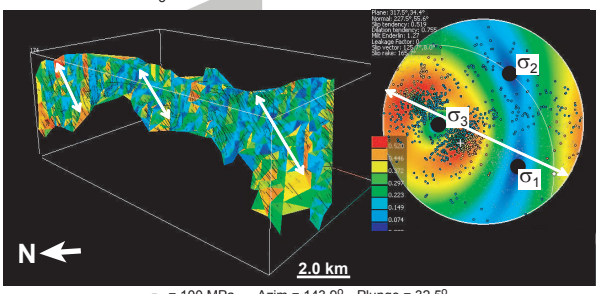

c)

σ_1 = 100 MPa Azim = 143.9° Plunge = 32.5°
σ_2 = 84.71 MPa Azim = 29.8° Plunge = 32.6°
σ_3 = 35.83 MPa Azim = 86.7° Plunge = -40.5°